Bioelectromagnetics 40:331–342 (2019)

Nonlinear Dispersive Model of Electroporation for Irregular Nucleated Cells

Michele Alessandro Chiapperino,[1] Pietro Bia,[2] Diego Caratelli,[3] Johan Gielis,[4] Luciano Mescia,[1]* Janja Dermol-Černe,[5] and Damijan Miklavčič[5]

[1]Department of Electrical and Information Engineering, Polytechnic University of Bari, Bari, Italy
[2]Department of Design Solution, Elettronica S.p.A, Rome, Italy
[3]Antenna Division, the Antenna Company, High Tech Campus, Eindhoven, The Netherlands
[4]Department of Bioengineering, University of Antwerp, Antwerp, Belgium
[5]Department of Biocybernetics, Faculty of Electrical Engineering, University of Ljubljana, Ljubljana, Slovenia

In this work, the electroporation phenomenon induced by pulsed electric field on different nucleated biological cells is studied. A nonlinear, non-local, dispersive, and space–time multiphysics model based on Maxwell's and asymptotic Smoluchowski's equations has been developed to calculate the transmembrane voltage and pore density on both plasma and nuclear membrane perimeters. The irregular cell shape has been modeled by incorporating in the numerical algorithm the analytical functions pertaining to Gielis curves. The dielectric dispersion of the cell media has been modeled considering the multi-relaxation Debye-based relationship. Two different irregular nucleated cells have been investigated and their response has been studied applying both the dispersive and non-dispersive models. By a comparison of the obtained results, differences can be highlighted confirming the need to make use of the dispersive model to effectively investigate the cell response in terms of transmembrane voltages, pore densities, and electroporation opening angle, especially when irregular cell shapes and short electric pulses are considered. Bioelectromagnetics. 2019;40:331–342. © 2019 Wiley Periodicals, Inc.

Keywords: cell membrane; pulsed electric field; electromagnetic modeling; dielectric dispersion; nucleated cells

INTRODUCTION

The biomembrane is a critical biological structure essential for cell function and survival as well as enabling separation between the cell interior from its extracellular environment controlling the exchange of molecules and nutrients. Moreover, it controls the flow of messages between cells by sending, receiving, and processing information in the form of chemical and electrical signals. When biomembranes are exposed to sufficiently intense pulsed electric fields (PEFs), the formation of transient aqueous pores improves membrane conductance and permeability, enhancing the ionic and molecular exchange between the cell and its environment [Pucihar et al., 2011; Kotnik et al., 2019]. This non-thermal electromagnetic phenomenon, known as electroporation (EP), is used in medical disease treatment to deliver drugs, vaccine, genes, and other molecules to mammalian cells [Yarmush et al., 2014].

The biomembranes' EP obtained using high intensity nanosecond PEF (nsPEF) is also used to disturb internal cellular structures such as nucleus, mitochondria, and endoplasmic reticulum. Depending on the duration and magnitude of applied pulses, the induced EP may cover more of the plasma membrane than the cell interior or it could affect the intracellular

Grant sponsors: Bando INNONETWORK-sostegno alle attività di R/&S per lo sviluppo di nuove tecnologie sostenibili, di nuovi prodotti e servizi plan: T-CARET eleassistenza e monitoraggio innovativi dei parametri vitali a domicilio con biosensori indossabili, project code: B37H17005210007 and Slovenian Research Agency (ARRS) (research core funding No. P2-0249, P3-0003, and IP-0510).

Conflicts of interest: None.

*Correspondence to: Luciano Mescia, Department of Electrical and Information Engineering, Polytechnic University of Bari, Via E. Orabona 4, 70125 Bari, Italy. E-mail: luciano.mescia@poliba.it

Received for review 10 May 2018; Accepted 3 May 2019

DOI:10.1002/bem.22197
Published online 9 June 2019 in Wiley Online Library (wileyonlinelibrary.com).

membranes more than the plasma one [Kotnik and Miklavčič, 2006; Pakhomov et al., 2014]. Moreover, nsPEF induces different physiological changes in mammalian cells leading to apoptosis in cancer cells [Xiao et al., 2013], the release of calcium from endoplasmic reticulum and calcium uptake from membranes outside [Pakhomova et al., 2014], caspase activation [Vernier et al., 2003a], externalization of phosphatidylserine (PS) [Vernier et al., 2006], calcium bursts [Vernier et al., 2003b], cytochrome C release [Napotnik et al., 2012], and DNA fragmentation [Beebe et al., 2003]. nsPEF also induces several effects on the nucleus such as alteration of its morphology [Napotnik et al., 2016], nuclear envelope damage with consecutive detachment of telomeres attached to the nuclear envelope [Stacey et al., 2011], alteration of nucleoplasm conductivity [Garner et al., 2007], and the enhancement of small nuclear ribonucleoprotein particle formation [Chen et al., 2007]. Different mathematical models of EP have been proposed in the literature to study pore formation in plasma, nuclear, and membranes of the organelles. These models can be classified as nonlinear with cell compartments treated as nondispersive media [Smith et al., 2006; Smith and Weaver, 2008; Pucihar et al., 2009; Rems et al., 2013; Retelj et al., 2013; Qiu et al., 2014; Yao et al., 2017] or linear with cell compartments treated as dispersive media [Denzi et al., 2013; Denzi et al., 2016]. However, in nanosecond pulse regime, the frequency-dependent dielectric properties of membranes and intracellular and extracellular media have to be considered to obtain an accurate and predictive EP model [Joshi and Hu, 2011; Denzi et al., 2016; Napotnik et al., 2016]. Moreover, in order to study the pore creation process inside the membranes, dielectric dispersion relationships pertaining to the cell media should be used in conjunction with the electroporation nonlinear model.

Nonlinear dispersive model of electroporation for a spherical single-shell cell was discussed in the literature [Pucihar et al., 2009; Salimi et al., 2013]. Different papers also illustrate the influence of the irregular shape of the membrane on the electroporation process [Pucihar et al., 2009; Qiu et al., 2014; Denzi et al., 2016]. In this paper, a nonlinear dispersive model of electroporation for nucleated irregular cells is presented. The nonlinear effect due to pore creation is considered in accordance to the asymptotic electroporation model based on Smolouchouski partial differential equation [Neu and Krassowska, 1999; Stewart et al., 2004; Lamberti et al., 2013]. The dielectric properties of biological cell media are described using the multi-relaxation Debye-based equation. By using a finite element-based technique, quasi-static Maxwell equations, and the Smolochowski partial differential equation and differential equation, relating the electric and polarization fields are simultaneously solved in the three-dimensional space-time domain. Moreover, the irregular cell shape has been modeled by Gielis' superformula [Gielis, 2003; Bia et al., 2015; Mescia et al., 2016]. Considering two types of nucleated cells, various simulations have been carried out to analyze the differences between the nonlinear dispersive and nondispersive models. By the simulation results, significant differences between the two analyzed models have been noticed. In particular, the difference is relevant in the case of the nucleated cell having an irregular plasma membrane shape. The noticeable discordance pointed out by the performed analysis is a compelling argument for the necessity of employing the dispersive dielectric properties in the model.

MATHEMATICAL MODELING

System Geometry

As illustrated in Figure 1, the biological system considered in the proposed studies is an axisymmetric cell constituted by the extracellular electrolyte (Ex), cytoplasm (Cp), nucleoplasm (Np), plasma (Pm), and

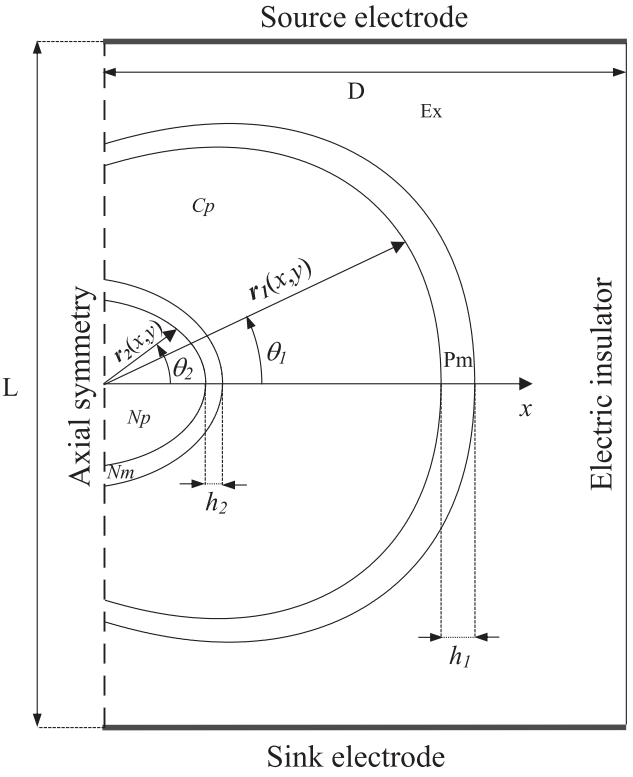

Fig. 1. Sketch of irregular nucleated biological cell exposed to uniform electric field.

nuclear (Nm) membranes. The applied pulsed electric field is generated by a couple of ideal planar electrodes placed on the top and lower ends of the computational domain. The irregular cell geometry is modeled by using the so-called Gielis superformula [Mescia et al., 2019]. In particular, the radius vectors describing the nuclear ($\mathbf{r}_1$) and plasma ($\mathbf{r}_2$) membranes are given by

$$\mathbf{r}_{1,2} = \hat{\mathbf{r}}_{1,2}\sqrt{x_{1,2}^2 + y_{1,2}^2} \tag{1}$$

where

$$x_{1,2} = A_{1,2}R_{1,2}(\theta)\cos\theta \tag{2}$$

$$y_{1,2} = B_{1,2}R_{1,2}(\theta)\sin\theta \tag{3}$$

$$R_1(\theta) = \left(\left|\frac{\cos(m_1\theta/4)}{a_1}\right|^{n_1} + \left|\frac{\sin(m_2\theta/4)}{a_2}\right|^{n_2}\right)^{-\frac{1}{b_1}} \tag{4}$$

$$R_2(\theta) = \left(\left|\frac{\cos(m_3\theta/4)}{a_3}\right|^{n_3} + \left|\frac{\sin(m_4\theta/4)}{a_4}\right|^{n_4}\right)^{-\frac{1}{b_2}} \tag{5}$$

with $\theta \in [-\pi/2, \pi/2]$, m_i, n_i, $i = 1,...,4$, and b_j, $j = 1, 2$ are positive real numbers, a_p, $p = 1,...,4$ are the strictly positive real numbers, $A_{1,2}$, $B_{1,2}$ are suitable scale factors.

DIELECTRIC RELAXATION MODEL

Considering that for several PEF applications the pulse spectral energy becomes significant at frequencies where dispersive effects occur, the developed numerical model takes into account the dielectric relaxation due to the time-dependent response of the dielectric media [Caratelli et al., 2016]. In particular, the dielectric properties of cell media are modeled by the multi-relaxation Debye dispersion equation:

$$\tilde{\varepsilon}(\omega) = \varepsilon_\infty + \sum_{i=1}^{N} \frac{\Delta\varepsilon_i}{1 + j\omega\tau_i} \tag{6}$$

where ε_∞ is the high frequency permittivity, N is the order of Debye dispersion process, $\Delta\varepsilon_i$ is the ith relaxation amplitude, and τ_i is the ith relaxation time. In detail, a second-order Debye equation is used to model the plasma and nuclear membranes, and a first order Debye equation is implemented to model the extracellular medium, cytoplasm, and nucleoplasm. Under the assumption that the coupling between the PEF and dielectric medium is weak, the linear response approximation effectively describes the dielectric polarization. For the homogeneous media characterizing the cell compartments, the linear response of the polarization vectors $\mathbf{P}_1$ and $\mathbf{P}_2$, corresponding to the first and second order Debye dispersion model, can be expressed in time domain as:

$$\mathbf{P}_{1,Ex} + \tau_{Ex}\frac{\partial\mathbf{P}_{1,Ex}}{\partial t} = (\Delta\varepsilon_{Ex} + \varepsilon_\infty - \varepsilon_0)\mathbf{E} + (\varepsilon_\infty - \varepsilon_0)\tau_{Ex}\frac{\partial\mathbf{E}}{\partial t} \tag{7}$$

$$\mathbf{P}_{1,Cp} + \tau_{Cp}\frac{\partial\mathbf{P}_{1,Cp}}{\partial t} = (\Delta\varepsilon_{Cp} + \varepsilon_\infty - \varepsilon_0)\mathbf{E} + (\varepsilon_\infty - \varepsilon_0)\tau_{Cp}\frac{\partial\mathbf{E}}{\partial t} \tag{8}$$

$$\mathbf{P}_{1,Np} + \tau_{Np}\frac{\partial\mathbf{P}_{1,Np}}{\partial t} = (\Delta\varepsilon_{Np} + \varepsilon_\infty - \varepsilon_0)\mathbf{E} + (\varepsilon_\infty - \varepsilon_0)\tau_{Np}\frac{\partial\mathbf{E}}{\partial t} \tag{9}$$

$$a_{2,Pm}\frac{\partial^2\mathbf{P}_{2,Pm}}{\partial t^2} + a_{1,Pm}\frac{\partial\mathbf{P}_{2,Pm}}{\partial t} + \mathbf{P}_{2,Pm} = b_{2,Pm}\frac{\partial^2\mathbf{E}}{\partial t^2} + b_{1,Pm}\frac{\partial\mathbf{E}}{\partial t} + b_{0,Pm}\mathbf{E} \tag{10}$$

$$a_{2,Nm}\frac{\partial^2\mathbf{P}_{2,Nm}}{\partial t^2} + a_{1,Nm}\frac{\partial\mathbf{P}_{2,Nm}}{\partial t} + \mathbf{P}_{2,Nm} = b_{2,Nm}\frac{\partial^2\mathbf{E}}{\partial t^2} + b_{1,Nm}\frac{\partial\mathbf{E}}{\partial t} + b_{0,Nm}\mathbf{E} \tag{11}$$

where

$$\begin{aligned} a_{1,Pm} &= \tau_{1,Pm} + \tau_{2,Pm} \\ a_{2,Pm} &= \tau_{1,Pm}\tau_{2,Pm} \\ b_{0,Pm} &= \Delta\varepsilon_{1,Pm} + \Delta\varepsilon_{2,Pm} + \varepsilon_\infty - \varepsilon_0 \\ b_{1,Pm} &= (\Delta\varepsilon_{2,Pm} + \varepsilon_\infty - \varepsilon_0)\tau_{1,Pm} + (\Delta\varepsilon_{1,Pm} + \varepsilon_\infty - \varepsilon_0)\tau_{2,Pm} \\ b_{2,Pm} &= (\varepsilon_\infty - \varepsilon_0)\tau_{1,Pm}\tau_{2,Pm} \end{aligned} \tag{12}$$

and

$$
\begin{aligned}
a_{1,Nm} &= \tau_{1,Nm} + \tau_{2,Nm} \\
a_{2,Nm} &= \tau_{1,Nm}\tau_{2,Nm} \\
b_{0,Nm} &= \Delta\varepsilon_{1,Nm} + \Delta\varepsilon_{2,Nm} + \varepsilon_\infty - \varepsilon_0 \\
b_{1,Nm} &= (\Delta\varepsilon_{2,Nm} + \varepsilon_\infty - \varepsilon_0)\tau_{1,Nm} + (\Delta\varepsilon_{1,Nm} + \varepsilon_\infty \\
&\quad - \varepsilon_0)\tau_{2,Nm} \\
b_{2,Nm} &= (\varepsilon_\infty - \varepsilon_0)\tau_{1,Nm}\tau_{2,Nm}
\end{aligned}
\tag{13}
$$

NONLINEAR MODEL

The pore densities for the plasma, N_{Pm}, and nuclear N_{Nm} membranes are calculated by using the asymptotic Smoluchowski equation [Krassowska and Filev, 2007]. In particular, their temporal evolutions are modeled by the following first-order partial differential equations:

$$
\frac{\partial N_{Pm}}{\partial t} = \alpha e^{\left(\Delta\Psi_{Pm}/V_{ep}\right)^2}\left[1 - \frac{N_{Pm}}{N_{eq}}e^{-q\left(\Delta\Psi_{Pm}/V_{ep}\right)^2}\right] \tag{14}
$$

$$
\frac{\partial N_{Nm}}{\partial t} = \alpha e^{\left(\Delta\Psi_{Nm}/V_{ep}\right)^2}\left[1 - \frac{N_{Nm}}{N_{eq}}e^{-q\left(\Delta\Psi_{Nm}/V_{ep}\right)^2}\right] \tag{15}
$$

where α is the rate coefficient describing the pore creation, $\Delta\Psi_{Pm}$ and $\Delta\Psi_{Nm}$ are the transmembrane voltage (TMV) for the plasma and nuclear membranes, respectively, V_{ep} is the characteristic voltage of electroporation, N_{eq} is the equilibrium pore density, and q is the EP constant. Considering the application of short pulses, the pore creation process dominates the pore expansion one, and the asymptotic model of electroporation can be used assuming that pores are created with constant radius of about 0.8 nm [Salimi et al., 2013].

Whenever the electroporation occurs, the formation of the pores in the cell membranes increases their conductivity. In particular, the average membrane conductivity is given by the sum of static membrane conductivity and contribution due to the electroporated part:

$$
\sigma_{Pm}(x, y, t) = \sigma_{0,Pm}(x, y, t) + \pi r_p^2 N_{Pm}(x, y, t)\sigma_{p,Pm}\frac{e^{v_{Pm}} - 1}{\frac{w_0 e^{w0-\eta v_{Pm}} - \eta v_{Pm}}{w_0 - \eta v_{Pm}}e^{v_{Pm}} - \frac{w_0 e^{w0+\eta v_{Pm}} + \eta v_{Pm}}{w_0 + \eta v_{Pm}}} \tag{16}
$$

$$
\sigma_{Nm}(x, y, t) = \sigma_{0,Nm}(x, y, t) + \pi r_p^2 N_{Nm}(x, y, t)\sigma_{p,Nm}\frac{e^{v_{Nm}} - 1}{\frac{w_0 e^{w0-\eta v_{Nm}} - \eta v_{Nm}}{w_0 - \eta v_{Nm}}e^{v_{Nm}} - \frac{w_0 e^{w0+\eta v_{Nm}} + \eta v_{Nm}}{w_0 + \eta v_{Nm}}} \tag{17}
$$

where $\sigma_{0,Pm}$ and $\sigma_{0,Nm}$ are the static plasma and nuclear membrane conductivity, $\sigma_{p,Pm}$ and $\sigma_{p,Nm}$ are the conductivity of the solution inside the pore for the plasma and nuclear membranes, respectively, r_p is the pore radius, w_0 is the pore energy barrier, η is the relative entrance length of pores, and ν_{Pm} and ν_{Nm} are the non-dimensional TMV for the plasma and nuclear membranes calculated using the following equations:

$$
\nu_{Pm} = \frac{q_e\,\Delta\Psi_{Pm}}{kT} \tag{18}
$$

$$
\nu_{Nm} = \frac{q_e\,\Delta\Psi_{Nm}}{kT} \tag{19}
$$

ELECTROMAGNETIC MODEL

The electric potential ϕ and electric field $\mathbf{E}$ are computed by neglecting time-variation of the magnetic field and solving in each cell subdomain the Laplace equation

$$
\nabla \cdot \frac{\partial}{\partial t}(\mathbf{P} - \varepsilon_0 \nabla\phi) + \nabla \cdot \sigma\nabla\phi = 0 \tag{20}
$$

in conjunction with the Equations (7–19) and the equation:

$$
\mathbf{E} = -\nabla\phi \tag{21}
$$

Moreover, the plasma TMV is calculated as the difference between the electric potential on the interior (i) and outer (o) sides of the plasma membrane:

$$
\Delta\Psi_{Pm}(x, y, t) = \phi_{\mathrm{i},Pm}(x, y, t) - \phi_{\mathrm{o},Pm}(x, y, t) \tag{22}
$$

The nuclear envelope is composed of two concentric lipid bilayers, forming the inner and outer nuclear membranes, separated by a perinuclear space of about 30-nm thickness. Moreover, the fluid in the perinuclear space can be considered to have conductivity value similar to that of the electrolyte in the cytoplasm. The inner and outer membranes are

thus electrically connected in series and taking into account that the cytoplasm conductivity is much higher than the membranes' conductivity, the voltage drop across the perinuclear space is negligible. By virtue of such matters, in our computations the nuclear envelope has been modeled as two lipid membranes in close contact between each other, each one having a thickness half of the nuclear envelope one. Moreover, we assumed that both membranes have the same electrical properties [Rems et al., 2013, Retelj et al., 2013]. In this way, the TMV is equally distributed between both membranes, allowing calculation of the TMV across one of the nuclear membranes as

$$\Delta\Psi_{Nm}(x, y, t) = \frac{\phi_{i,Ne}(x, y, t) - \phi_{o,Ne}(x, y, t)}{2} \tag{23}$$

where $\phi_{i,Ne}(x,y,t)$ and $\phi_{o,Ne}(x,y,t)$ are the electric potential on the interior and outer sides of the nuclear envelope, respectively.

The electrical boundary conditions pertaining to the source and sink electrodes were set to $\phi = V(t)$ and $\phi = 0$, respectively, $V(t)$ being the PEF signal constructed using smoothed piecewise function consisting of unipolar pulse. The study was performed using a direct solver managing a large sparse linear system of equations with good memory efficiency. The solver uses LU decomposition to compute the system solution and a pre-ordering algorithm that permutes the columns of the system matrix minimizing the number of non-zeros in the L and U factors. A free time-stepping algorithm was utilized to enable the solver to freely select the time steps during the computation (Table 1).

NUMERICAL RESULTS AND DISCUSSION

The model has been validated by comparing the results concerning the nucleated spherical cell simulations with the literature ones. In particular, the temporal evolution of plasma membrane $\Delta\Psi_m$ and pore density shown in Figure 2 have been compared with the corresponding curves reported in Lamberti et al. [2013]. In the comparison analysis a pore radius $r_p = 3.5$ nm has been considered. Moreover, with the aim to perform a right validation test the cell biological media are non-dispersive as in Lamberti et al. [2013]. Figure 2a shows the temporal evolution of the plasma membrane $\Delta\Psi_m$ at the top of the cell ($\theta = 90°$) when a PEF having amplitude $E = 2.5$ MV/m, pulse duration $T = 50$ ns, rise time $t_r = 30$ ns, and fall time $t_f = 30$ ns is applied to the external electrodes. In Figure 2b the time behavior of the plasma membrane pore density at

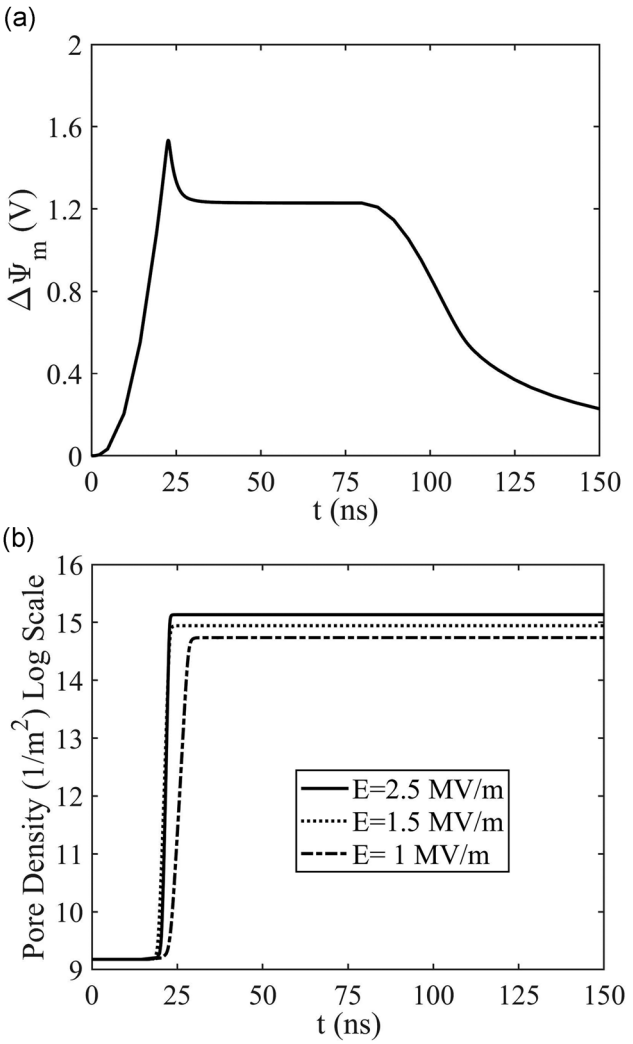

Fig. 2. Temporal evolution of (a) plasma membrane TMV at the top of the nucleated spherical cell ($\theta = 90°$) for $r_p = 3.5$ nm. Applied voltage signal having amplitude $E = 2.5$ MV/m, pulse duration $T = 50$ ns, rise time $t_r = 30$ ns, and fall time $t_f = 30$ ns. Temporal evolution of (b) plasma membrane pore density at the top of the nucleated spherical cell ($\theta = 90°$) for $r_p = 3.5$ nm, when three different voltage signals are applied: $E = 2.5$ MV/m, pulse duration $T = 50$ ns, rise time $t_r = 30$ ns, and fall time $t_f = 30$ ns; $E = 1.5$ MV/m, pulse duration $T = 50$ ns, rise time $t_r = 18$ ns and fall time $t_f = 18$ ns; $E = 1$ MV/m, pulse duration $T = 50$ ns, rise time $t_r = 12$ ns, and fall time $t_f = 12$ ns.

TABLE 1. Definition of Acronyms

Abbreviations	Definition
EP	Electroporation
PEF	Pulsed electric field
EPRL	Electroporation relative length

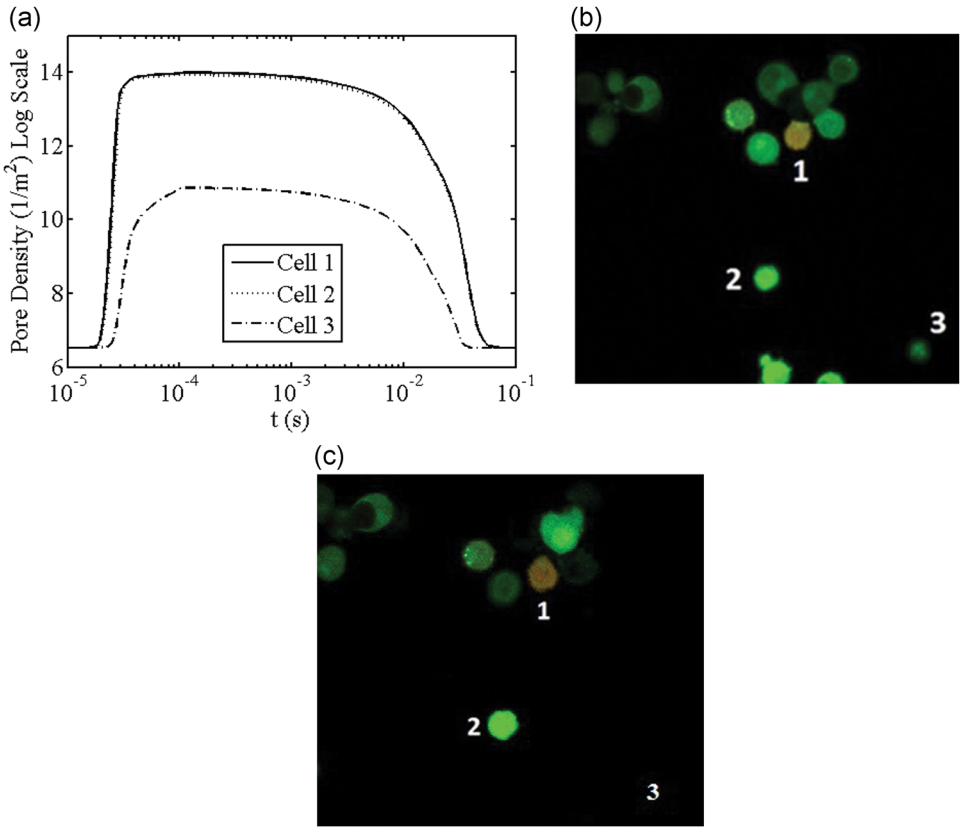

Fig. 3. (a) Temporal evolution of pore density evaluated in the points of maximum for three different real cells. Images regarding the experimental results: (b) cells before electroporation, (c) electroporated cells. Rectangular unipolar pulse type, voltage amplitude 60 V, duration $T = 100$ μs, time windows 0.1 s.

the top of the cell is reported when the previous voltage signal and two further voltage stresses with the following pulse parameters are applied: $E = 1.5$ MV/m, pulse duration $T = 50$ ns, rise time $t_r = 18$ ns, and fall time $t_f = 18$ ns; $E = 1$ MV/m, pulse duration $T = 50$ ns, rise time $t_r = 12$ ns, and fall time $t_f = 12$ ns. The obtained results are in good agreement with the corresponding ones reported in Lamberti et al. [2013], which in turn have been used to provide an exhaustive explanation of the experimental results concerning the effects induced by nsPEF on Jurkat cells. In fact, the pore density relative error between the literature and the present models is about 5% for all the pulse voltages. The differences between the two models could be mainly due to the different time domain solvers, time step, and spatial discretization of the computational domain. The model has also been validated using preliminary experimental results pertaining to real cells exposed to a rectangular unipolar pulse having voltage amplitude of 60 V and duration of 100 μs. Figure 3a shows the temporal evolution of pore density evaluated at the corresponding maximum points for the three different real cells. In particular, the electroporated cells resulting from the numerical investigation correspond to those observed experimentally by detecting the red and green fluorescence (see Fig. 3c) due to the influx of calcium in the cytoplasm. In particular, by an inspection of Figures 3a and c, it is worthwhile to note that cell 1 and cell 2 are both electroporated and cell 3 does not appear in microphotograph since it is not electroporated. As result, a good agreement between the numerical and experimental results can be inferred. Instead, Figure 3b shows all the cells before electroporation. Furthermore, the present model has also been previously validated for the case of spherical non-nucleated cells [Mescia et al., 2018]. Using the numerical model previously described, the electroporation process has been studied for two types of cells: prolate spheroid and muscular-like. The cells are bounded by a cylindrical computational domain having radius and height equal to 100 μm. Table 2 summarizes the polarization, geometric, electric,

TABLE 2. Polarization, Electric, Geometrical and Electroporation Parameters

Symbol	Value	Description
τ_1^{Pm}	$3 \times 10^{-9}s$	First relaxation time of plasma membrane [Klosgen et al., 1996]
τ_1^{Nm}	$3 \times 10^{-9}s$	First relaxation time of nuclear membrane [Klosgen et al., 1996]
τ_2^{Pm}	$4.6 \times 10^{-10}s$	Second relaxation time of plasma membrane [Klosgen et al., 1996]
τ_2^{Nm}	$4.6 \times 10^{-10}s$	Second relaxation time of nuclear membrane [Klosgen et al., 1996]
τ_{Ex}	$6.2 \times 10^{-12}s$	Relaxation time of extracellular medium [Kotnik and Miklavčič, 2000]
τ_{Cp}	$6.2 \times 10^{-12}s$	Relaxation time of cytoplasm [Kotnik and Miklavčič, 2000]
τ_{Np}	$6.2 \times 10^{-12}s$	Relaxation time of nucleoplasm [Kotnik and Miklavčič, 2000]
$\Delta\varepsilon_1^{Pm}$	$2.3 \times 10^{-11}F/m$	First relaxation amplitude of plasma membrane [Klosgen et al., 1996]
$\Delta\varepsilon_1^{Nm}$	$2.3 \times 10^{-11}F/m$	First relaxation amplitude of nuclear membranes [Klosgen et al., 1996]
$\Delta\varepsilon_2^{Pm}$	$7.4 \times 10^{-12}F/m$	Second relaxation amplitude of plasma membrane [Klosgen et al., 1996]
$\Delta\varepsilon_2^{Nm}$	$7.4 \times 10^{-12}F/m$	Second relaxation amplitude of nuclear membrane [Klosgen et al., 1996]
$\Delta\varepsilon_{Ex}$	$5.9 \times 10^{-10}F/m$	Relaxation amplitude of extracellular medium [Kotnik and Miklavčič, 2000]
$\Delta\varepsilon_{Cp}$	$5.9 \times 10^{-10}F/m$	Relaxation amplitude of cytoplasm [Kotnik and Miklavčič, 2000]
$\Delta\varepsilon_{Np}$	$5.9 \times 10^{-10}F/m$	Relaxation amplitude of nucleoplasm [Kotnik and Miklavčič, 2000]
ε_∞	$13.9 \times 10^{-12}F/m$	High frequency permittivity [Klosgen et al., 1996]
ε_0	$8.85 \times 10^{-12}F/m$	Dielectric permittivity of vacuum
ε_r^{Ex}	72	Relative permittivity of extracellular medium [Salimi et al., 2013]
ε_0^{Pm}	5	Static relative permittivity of plasma membrane [Salimi et al., 2013]
ε_r^{Cp}	72	Relative permittivity of cytoplasm [Salimi et al., 2013]
ε_0^{Nm}	7	Static relative permittivity of nuclear membrane [Rems et al., 2013]
ε_r^{Np}	72	Relative permittivity of nucleoplasm [Rems et al., 2013]
σ_{Ex}	$1.2\ S/m$	Conductivity of the extracellular medium [Salimi et al., 2013]
σ_0^{Pm}	$9.5 \times 10^{-9}S/m$	Passive conductivity of the plasma membrane [Salimi et al., 2013]
σ_{Cp}	$0.3\ S/m$	Conductivity of cytoplasm [Salimi et al., 2013]
σ_0^{Nm}	$1 \times 10^{-4}S/m$	Passive conductivity of the nuclear membrane [Rems et al., 2013]
σ_{Np}	$0.6\ S/m$	Conductivity of nucleoplasm [Rems et al., 2013]
σ_p^{Pm}	$0.6492\ S/m$	Conductivity of the solution inside the pore for the plasma membrane [Rems et al., 2013]
σ_p^{Nm}	$0.4328\ S/m$	Conductivity of the solution inside the pore for the nuclear membrane [Rems et al., 2013]
r_p	$0.8nm$	Pore radius [Salimi et al., 2013]
α	$10^9 m^{-2}s^{-1}$	Pore creation rate density [Salimi et al., 2013]
V_{ep}	$224mV$	Characteristic voltage of electroporation [Salimi et al., 2013]
N_{eq}	$3.3 \times 10^6 m^{-2}$	Equilibrium pore density [Salimi et al., 2013]
w_0	3.2	Energy barrier inside the pore [Salimi et al., 2013]
η	0.15	Relative length of pore entrance area [Salimi et al., 2013]
q	1	EP constant [Salimi et al., 2013]
q_e	$1.65 \times 10^{-19}C$	Electron electric charge
K	$1.38 \times 10^{-23}J/K$	Boltzmann constant
T	$295K$	Temperature
h_{Pm}	$5nm$	Plasma membrane thickness [Rems et al., 2013]
h_{Ne}	$10nm$	Nuclear envelope thickness [Rems et al., 2013]

and electroporation parameters used in numerical simulations. Our computations and data plots have been performed using COMSOL Multiphysics 5.3 (COMSOL, Stockholm, Sweden) and MATLAB R2018b suite software (MathWorks, Natick, MA).

The first type of cell has a prolate spheroid shape (see Fig. 4a), characterized by semi-axis $a_1 = 2\,\mu$m and $b_1 = 7.5\,\mu$m, for the plasma membrane, and semi-axis $a_2 = 0.75\,\mu$m and $b_2 = 1.5\,\mu$m, for the nuclear membrane. The thickness of plasma membrane and nuclear envelope are $h_{Pm} = 5$ nm and $h_{Ne} = 10$ nm, respectively. In physiological conditions the nuclear envelope has a relatively high conductivity value compared to that of the plasma membrane. This is to be expected because of the large number of electrolyte-filled nuclear pores that penetrate the inner and outer nuclear membranes. So, in our calculation the plasma and nuclear membrane conductivities are $\sigma_0^{Pm} = 9.5 \times 10^{-9}$S/m and $\sigma_0^{Nm} = 1 \times 10^{-4}$ S/m, respectively. The cells are exposed to a PEF having rectangular shape with amplitude $E = 100$ kV/cm, duration $T = 10$ ns, rise time $t_r = 0.9$ ns, and fall time $t_f = 0.9$ ns. All results refer to both plasma dispersive (D_{Pm}) and nuclear dispersive (D_{Nm}) membranes as

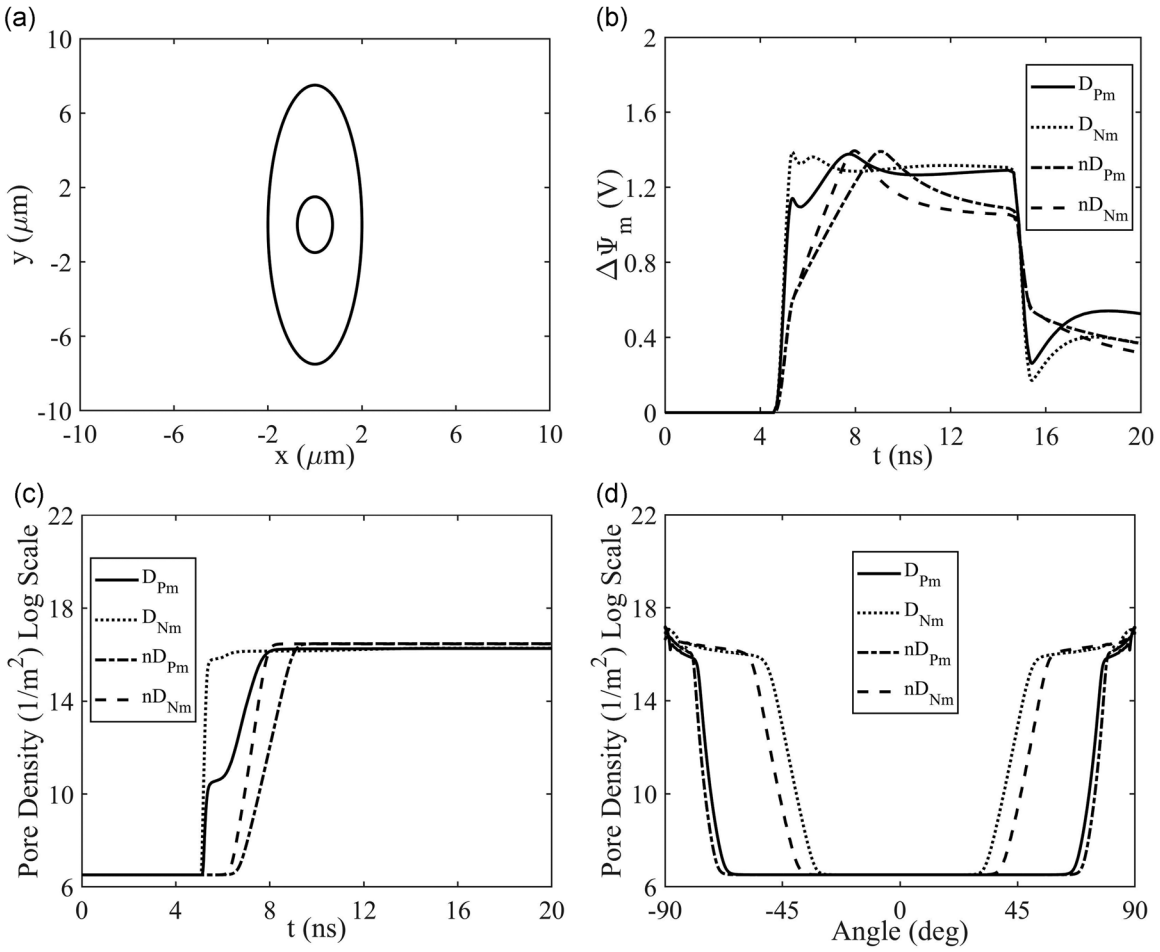

Fig. 4. Nucleated biological cell with prolate spheroidal shape (a), results for plasma (Pm) and nuclear (Nm) membranes obtained using the dispersive (D) and non-dispersive (nD) model: (b) Temporal evolution of TMVand (c) pore density at the top of the cell ($\theta = 90°$), (d) pore density versus the polar angle at $t = 20$ ns. Pulse amplitude and duration equal to 100 kV/cm and 10 ns, respectively.

well as to plasma non-dispersive (nD_{Pm}) and nuclear non-dispersive (nD_{Nm}) membrane models. Figures 4b and c show the time response of the TMV and pore density at the top of the spheroidal cell. As shown in Figures 4b and c and in accordance with results reported in Salimi et al. [2013], the increase of the TMV and resulting activation of electroporation occur faster in the dispersive model. This is due to the membrane-charging time constants, characterizing the dispersive model, which are significantly smaller than that of the non-dispersive one. As a consequence of the external pulse application, the TMV on the plasma and nuclear membranes increases approximately to 1.4 V, both for the dispersive and non-dispersive model. However, the enhancement of pore density in the plasma and nuclear membranes generates a fast increase of membrane conductivity leading to a TMV decrease. For both the dispersive and non-dispersive models, the nuclear membrane is electroporated before the plasma membrane. The explanation of this phenomenon is related to the fact that the charging time constant of nuclear membrane is less than that of the plasma membrane [Schoenbach et al., 2007]. This effect is more prominent when shorter pulses are used, as in our case. Figure 4d reports the pore density around the cell perimeter at time instant $t = 20$ ns, and a relevant difference is evaluated between the dispersive and non-dispersive model. In particular, the electroporation relative length (EPRL), i.e., the ratio between the length of the electroporated region and the total length of the cell membrane, pertaining to the plasma membrane and calculated using the dispersive model, is about 2.5% higher than that calculated using a non-dispersive one. Moreover, the EPRL of the nuclear membrane calculated using the dispersive model is about

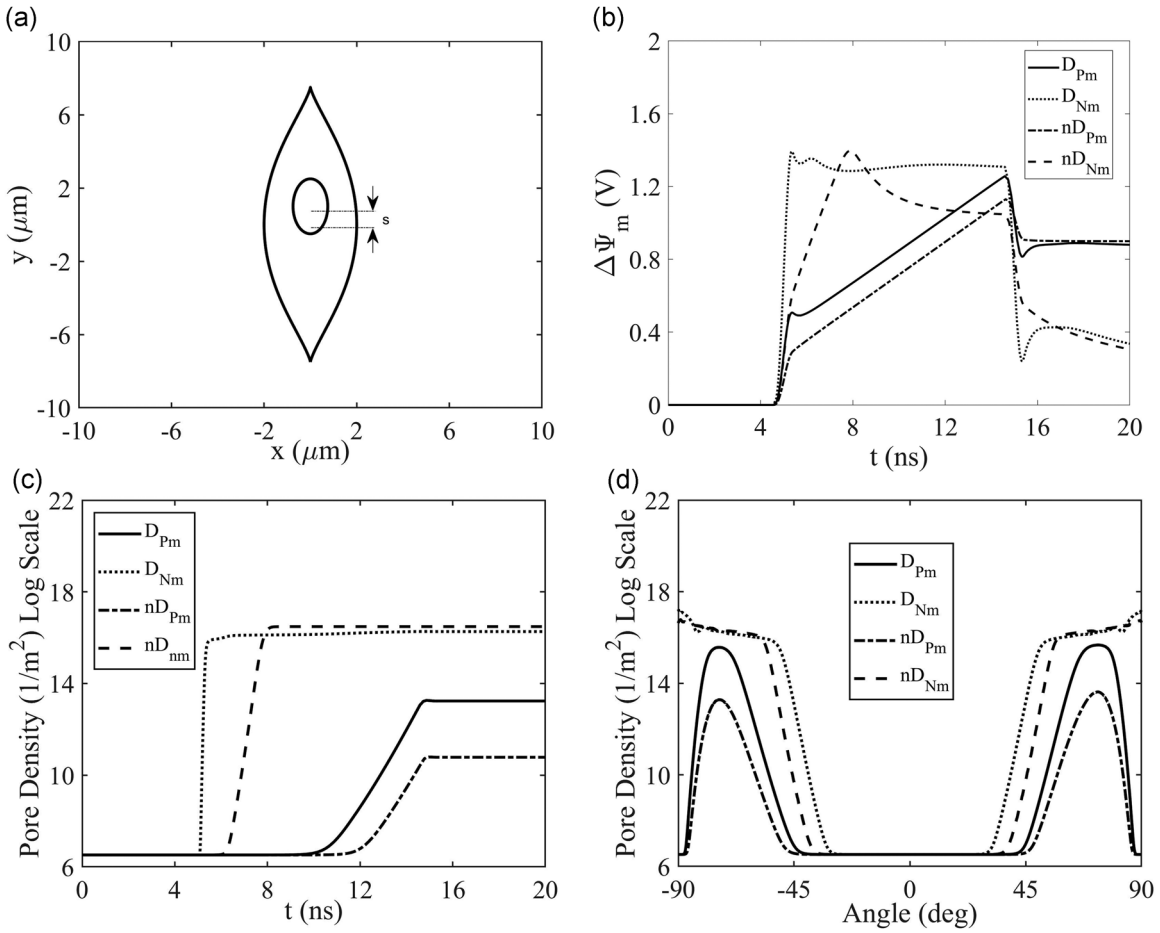

Fig. 5. Smooth muscular cell with shifted nucleus (a), results for plasma (Pm) and nuclear (Nm) membranes obtained using the dispersive (D) and non-dispersive (nD) model: (b) Temporal evolution of TMVand (c) pore density for $\theta = 75°$, (d) pore density versus the polar angle at $t = 20\ ns$. Pulse amplitude and duration equal to 100 kV/cm and 10 ns, respectively.

7.3% higher than that calculated using the non-dispersive one. To evaluate the EPRL, the cell membranes are considered to be significantly electroporated when the pore density reaches a value of $10^{14}\,\mathrm{m}^{-2}$ [Retelj et al., 2013].

The second analyzed nucleated cell is the muscular-like one reported in Figure 5a. For this type of cell, the shape of the plasma membrane has been modeled using the Gielis superformula parameters $m_1 = m_2 = 2$, $n_1 = n_2 = 0.8$, $d_1 = d_2 = 1$, $b_1 = 0.6$ [Mescia et al., 2018]. The spatial scale factors are $A_1 = 4\,\mu\mathrm{m}$ and $B_1 = 7.5\ \mu\mathrm{m}$. The nucleus has prolate spheroid shape with semi-axis $a_2 = 0.75\ \mu\mathrm{m}$ and $b_2 = 1.5\ \mu\mathrm{m}$ and center shifted of $s = 1\ \mu\mathrm{m}$ in respect to the origin. Figures 5b and c show the time response of the $\Delta\Psi_\mathrm{m}$ and pore density at the angular place $\theta = 75°$ for both plasma and nuclear membranes, obtained using the dispersive and non-dispersive model. Also in this case, the activation of electroporation occurs faster in the dispersive model. In accordance with the nucleated prolate spheroidal cell, also for the nucleated muscular-like cell, the nuclear membrane is electroporated before the plasma membrane for both the dispersive and non-dispersive model. However, with respect to the prolate spheroid cell a different angle at which the results are shown is considered. In fact, as shown in Figure 4d, in the prolate spheroid cell the plasma membrane is not significantly electroporated for $\theta = 75°$. Instead, the electroporation is maximal for $\theta = 90°$, corresponding to the plots of Figures 4b and c, in both nuclear and plasma membranes. On the contrary, in the muscular-like cell the plasma membrane is not electroporated for $\theta = 90°$ and exhibits the maximum electroporation value at the angle $\theta = 75°$, corresponding to the plots of Figures 5b and c. For this reason, we analyzed

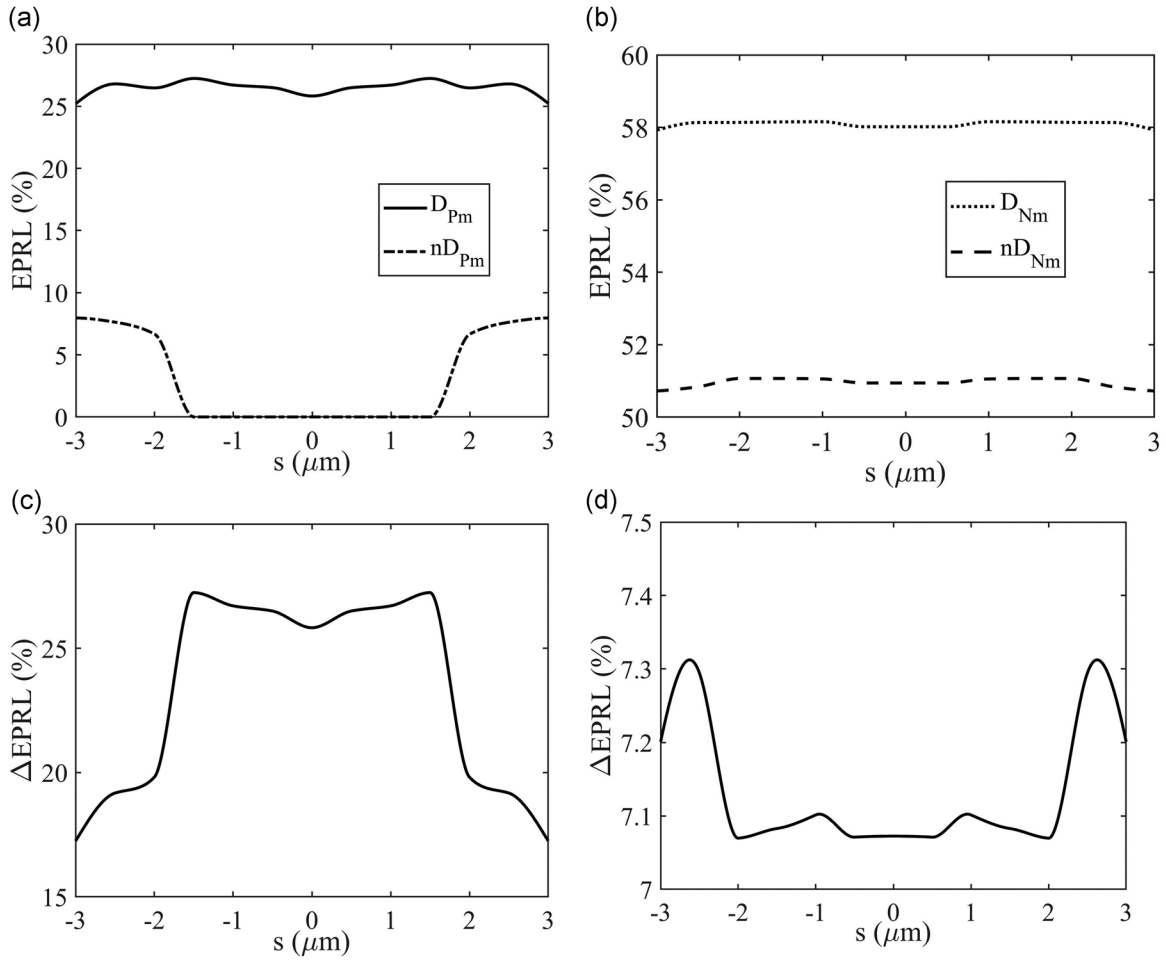

Fig. 6. Nucleus decentralization parametric study: (a) *EPRL* for plasma membrane (Pm) and (b) *EPRL* for nuclear membrane (Nm) versus the nucleus decentralization parameter *s*, obtained using the dispersive (D) and non-dispersive (nD) model. Absolute difference between the dispersive and non-dispersive *EPRL* versus the nucleus decentralization parameter *s* for (c) plasma membrane and for (d) nuclear membrane. Computations performed at time instant $t = 20$ ns.

the results at different angles. Again, as shown in Figure 5b, the TMV curves have a very different behavior. In fact, due to the different shape, size, and thickness as well as the different conductivity and permittivity of the nuclear and plasma membranes, they are stimulated in a different way by the electric pulse. As reported in Figures 5c and d, a significant difference is evaluated between the two analyzed models. For this type of cell, the difference between the two models is magnified by the irregular geometrical shape of the plasma membrane. At $\theta = 75°$ only the nuclear membrane is significantly electroporated for both dispersive and non-dispersive models. From Figure 5d, a significant absolute difference between the dispersive and non-dispersive EPRL for both the membranes can be inferred. In particular, the EPRL difference is about 26.7% for the plasma membrane, and about 7.1% for the nuclear membrane.

To investigate the influence of the nucleus shift on the EP process, a parametric study has been carried out. The aim of this study is to evaluate the electroporation phenomenon in a more complicated geometrical configuration and to emphasize that the discrepancy between the dispersive and non-dispersive models is further magnified by this new geometry framework. Also in this case, the analysis has been performed for plasma and nuclear membranes, using both the dispersive and non-dispersive models. Figures 6a and b illustrate, respectively, the EPRL for plasma and nuclear membranes as functions of the nucleus shift s, calculated using the dispersive (D) and non-dispersive (nD) model. The plasma EPRL calculated using the dispersive model changes within

limited values ranging from 25% to 27%. Instead, the plasma EPRL evaluated using the non-dispersive model is zero for s ranging from -1.5 μm to 1.5 μm and increases to about 8% moving the nucleus towards the electrodes. Thus, the plasma EPRL evaluated using the non-dispersive shows a dependence on the position of the nucleus. In particular, with respect to the non-dispersive model, lower high-frequency membrane permittivity characterizing the dispersive model results in a higher TMV. As a consequence, in the non-dispersive case a lack of plasma electroporation for s ranging from -1.5 μm to 1.5 μm occurs. For the nuclear membranes, the EPRL calculated using the dispersive and non-dispersive model is quite constant and equal to about 58% and 51%, respectively. As shown in Figure 6c, the absolute difference between EPRL of plasma membrane calculated using the dispersive and non-dispersive models has a minimum of about 17.2% at $s = \pm 3$ μm reaching the maximum value of about 27.2% close to $s = \pm 1.5$ μm. A local minimum of about 25.8% is evident at $s = 0$ μm. Figure 6d shows that for the nuclear membrane, the absolute difference between the dispersive and non-dispersive EPRL changes in the range 7%/7.3%.

CONCLUSION

In this paper, a nonlinear dielectric dispersion mathematical model of electroporation for real-like shape nucleated cells is developed. The presented model solves Maxwell's equations in conjunction with the Smolouchouski partial differential equation, which describes the nonlinear pore dynamics creation. The dielectric dispersion properties of each cell compartment are considered using the Debye dispersion model. Finally, the Gielis superformula has been integrated in the model to describe the irregular geometry of the cell to analyze.

Considering the nucleated prolate spheroidal cell and smooth muscular cell with shifted nucleus, various simulations have been performed with the aim to investigate the differences between the nonlinear dispersive model and nonlinear non-dispersive model. Starting from the prolate spheroidal cell, an absolute difference between the dispersive and non-dispersive EPRL of 2.55% for the plasma membrane and 7.33% for the nuclear membrane are obtained. This difference increases with the irregular geometrical shape of the plasma membrane.

In particular, for the muscular-like cell with the nucleus shifted along the y axis of $s = 1$ μm, EPRL is, respectively, 26.70% for the plasma membrane and 7.10% for the nuclear membrane. Finally, a parametric analysis has been carried out, to evaluate the absolute difference between the dispersive and non-dispersive EPRL as functions of the shift parameter s. A $\Delta EPRL$ ranging between 17.25% and 27.24% for the plasma membrane and between 7.07% and 7.31% for the nuclear membrane is obtained. However, by an inspection of the obtained results it is possible to conclude that for real-like cells, a relevant difference is observed between the nonlinear dispersive model and nonlinear nondispersive model. Then, the presented numerical model combining the real geometry description, accurate dielectric dispersion response of the exposed cell, and nonlinear behavior of the EP process provides a realistic and detailed analysis of electroporation process.

ACKNOWLEDGMENTS

We would like to thank Dr. M. Čemažar and B. Starešinič from the Institute of Oncology Ljubljana, Slovenia, for their help with in vitro cell experiments and microscopy.

REFERENCES

Beebe SJ, White J, Blackmore PF, Deng Y, Somers K, Schoenbach KH. 2003. Diverse effects of nanosecond pulsed electric fields on cells and tissues. DNA Cell Biol 22:785–796.

Bia P, Caratelli D, Mescia L, Gielis J. 2015. Analysis and synthesis of supershaped dielectric lens antennas. IET Microw Antennas Propag 9:1497–1504.

Caratelli D, Mescia L, Bia P, Stukach OV. 2016. Fractional-calculus-based FDTD algorithm for ultrawideband electromagnetic characterization of arbitrary dispersive dielectric materials. IEEE Trans Antennas Propag 64:3533–3544.

Chen N, Garner AL, Chen G, Jing Y, Deng Y, Swanson RJ, Kolb JF, Beebe SJ, Joshi RP, Schoenbach KH. 2007. Nanosecond electric pulses penetrate the nucleus and enhance speckle formation. Biochem Biophys Res Commun 364:220–225.

Denzi A, Camera F, Merla C, Benassi B, Consales C, Paffi A, Apollonio F, Liberti M. 2016. A microdosimetric study of electropulsation on multiple realistically shaped cells: effect of neighbours. J Membr Biol 249:691–701.

Denzi A, Merla C, Camilleri P, Paffi A, d'Inzeo G, Apollonio F, Liberti M. 2013. Microdosimetric study for nanosecond pulsed electric fields on a cell circuit model with nucleus. J Membr Biol 246:761–767.

Garner AL, Chen G, Chen N, Sridhara V, Kolb JF, Swanson RJ, Beebe SJ, Joshi RP. 2007. Ultrashort electric pulse induced changes in cellular dielectric properties. Biochem Biophys Res Commun 362:139–144.

Gielis J. 2003. A generic geometric transformation that unifies a wide range of natural and abstract shapes. Am J Bot 90:333–338.

Joshi RP, Hu Q. 2011. Case for applying subnanosecond high-intensity, electrical pulses to biological cells. IEEE Trans Biomed Eng 58:2860–2866.

Klosgen B, Reichle C, Kohlsmann S, Kramer KD. 1996. Dielectric spectroscopy as a sensor of membrane headgroup mobility and hydration. Biophys J 71:3251–3260.

Kotnik T, Miklavčič D. 2000. Theoretical evaluation of the distributed power dissipation in biological cells exposed to electric fields. Bioelectromagnetics 21:385–394.

Kotnik T, Miklavčič D. 2006. Theoretical evaluation of voltage inducement on internal membranes of biological cells exposed to electric fields. Biophys J 90(2), 480–491.

Kotnik T, Rems L, Tarek M, Miklavčič D. 2019. Membrane electroporation and electropermeabilization: mechanisms and models. Ann Rew Biophys 48:63–91.

Krassowska W, Filev PD. 2007. Modeling electroporation in a single cell. Biophys J 92:404–417.

Lamberti P, Tucci V, Romeo S, Sannino A, Scarfi MR, Zeni O. 2013. nsPEF-induced effects on cell membranes: use of electrophysical model to optimize experimental design. IEEE Trans Dielectr Electr Insul 20:1231–1238.

Mescia L, Bia P, Caratelli D, Chiapperino MA, Stukach O, Gielis J. 2016. Electromagnetic mathematical modeling of 3D super-shaped dielectric lens antennas. Math Prob Eng 2016:1–10.

Mescia L, Chiapperino MA, Bia P, Gielis J, Caratelli D. 2018. Modeling of electroporation induced by pulsed electric fields in irregularly shaped cells. IEEE Trans Biomed Eng 65:414–423.

Mescia L, Chiapperino MA, Bia P, Lamacchia CM, Gielis J, Caratelli D. 2019. Design of electroporation process in irregularly shaped multicellular systems. Electronics 8:1–17.

Napotnik TB, Reberšek M, Vernier PT, Mali B., Miklavčič D. 2016. Effects of high voltage nanosecond electric pulses on eukaryotic cells (in vitro): A systematic review. Bioelechem 110:1–12.

Napotnik TB, Wu YH, Gundersen MA, Miklavčič D, Vernier PT. 2012. Nanosecond electric pulses cause mitochondrial membrane permeabilization in jurkat cells. Bioelectromagnetics 33:257–264.

Neu JC, Krassowska W. 1999. Asymptotic model of electroporation. Phys Rev E 59:3471–3482.

Pakhomov AG, Semenov I, Xiao S, Pakhomova ON, Gregory B, Schoenbach KH, Ullery JC, Beier HT, Rajulapati SR, Ibey BL. 2014. Cancellation of cellular responses to nanoelectroporation by reversing the stimulus polarity. Cell Mol Life Sci 71:4431–4441.

Pakhomova ON, Gregory B, Semenov I, Pakhomov AG. 2014. Calcium-mediated pore expansion and cell death following nanoelectroporation. Biochim Biophys Acta 1838:2547–2554.

Pucihar G, Krmelj J, Rebersek M, Napotnik TB, Miklavčič D. 2011. Equivalent pulse parameters for electroporation. IEEE Trans Biomed Eng 58:3279–3288.

Pucihar G, Miklavčič D, Kotnik T. 2009. A time-dependent numerical model of transmembrane voltage inducement and electroporation of irregularly shaped cells. IEEE Trans Biomed Eng 56:1491–1501.

Qiu H, Xiao S, Joshi RP. 2014. Simulations of voltage transients across intracellular mitochondrial membranes due to nanosecond electrical pulses. IEEE T Plasma Sci 42:3113–3120.

Rems L, Ušaj M, Kandušer M, Reberšek M, Miklavčič D, Pucihar G. 2013. Cell electrofusion using nanosecond electric pulses. Sci Rep 3:1–10.

Retelj L, Pucihar G, Miklavčič D. 2013. Electroporation of intracellular liposomes using nanosecond electric pulses—a theoretical study. IEEE Trans Biomed Eng 60:2624–2635.

Salimi E, Thomson DJ, Bridges GE. 2013. Membrane dielectric dispersion in nanosecond pulsed electroporation of biological cells. IEEE Trans Dielectr Electr Insul 20:1256–1265.

Schoenbach KH, Hargrave B, Joshi RP, Kolb JF, Nuccitelli R, Osgood C, Pakhomov A, Stacey M, Swanson RJ, White JA, Xiao S, Zhang J, Beebe SJ, Blackmore PF, Buescher ES. 2007. Bioelectric effects of intense nanosecond pulses. IEEE Trans Dielect Electr Insul 14:1088–1109.

Smith KC, Gowrishankar TR, Esser AT, Stewart DA, Weaver JC. 2006. The spatially distributed dynamic transmembrane voltage of cells and organelles due to 10-ns pulses: meshed transport networks. IEEE Trans Plasma Sci 34:1394–1404.

Smith KC, Weaver JC. 2008. Active mechanisms are needed to describe cell responses to submicrosecond, megavolt-permeter pulses: cell models for ultrashort pulses. Biophys J 95:1547–1563.

Stacey M, Fox P, Buescher S, Kolb J. 2011. Nanosecond pulsed electric field induced cytoskeleton, nuclear membrane and telomere damage adversely impact cell survival. Bioelectrochemistry 82:131–134.

Stewart DA, Jr., Gowrishankar TR, Weaver JC. 2004. Transport lattice approach to describing cell electroporation: use of a local asymptotic model. IEEE Trans Plasma Sci 32:1696–1708.

Vernier PT, Li A, Marcu L, Craft CM, Gundersen MA. 2003a. Ultrashort pulsed electric fields induce membrane phospholipid translocation and caspase activation: differential sensitivities of jurkat T lymphoblasts and rat glioma C6 cells. IEEE Trans Dielectr and Electr Insul 10:795–809.

Vernier PT, Sun Y, Marcu L, Salemi S, Craf CM, Gundersena MA. 2003b. Calcium bursts induced by nanosecond electric pulses. Biochem Biophys Res Commun 310:286–295.

Vernier PT, Ziegler MJ, Sun Y, Chang WV, Gundersen MA, Tieleman DP. 2006. Nanopore formation and phosphatidylserine externalization in a phospholipid bilayer at high transmembrane potential. J Am Chem Soc 128: 6288–6289.

Xiao D, Yao C, Liu H, Li C, Cheng J, Guo F, Tang L. 2013. Irreversible electroporation and apoptosis in human liver cancer cells induced by nanosecond electric pulses. Bioelectromagnetics 34:512–520.

Yao C, Liu H, Zhao Y, Mi Y, Dong S, Lv Y. 2017. Analysis of dynamic processes in single-cell electroporation and their effects on parameter selection based on the finite-element model. IEEE Trans Plasma Sci 45:889–900.

Yarmush ML, Golberg A, Sersa G, Kotnik T, Miklavcic D. 2014. Electroporation-based technologies for medicine: principles, applications and challenges. Annu Rev Biomed Eng 16:295–320.